Mathematical and Computational Applications

MDPI

Article

Numerical Study of the Effect of a Heated Cylinder on Natural Convection in a Square Cavity in the Presence of a Magnetic Field

Muhammad Sajjad Hossain [1,*], Muhammad Fayz-Al-Asad [2], Muhammad Saiful Islam Mallik [1], Mehmet Yavuz [3,*], Md. Abdul Alim [2] and Kazi Md. Khairul Basher [4]

[1] Department of Arts and Sciences, Faculty of Engineering, Ahsanullah University of Science and Technology (AUST), Dhaka 1208, Bangladesh; saiful_math.as@aust.edu
[2] Department of Mathematics, Bangladesh University of Engineering and Technology (BUET), Dhaka 1000, Bangladesh; fayzmath.buet@gmail.com (M.F.-A.-A.); maalim@math.buet.ac.bd (M.A.A.)
[3] Department of Mathematics and Computer Sciences, Faculty of Science, Necmettin Erbakan University, Konya 42090, Türkiye
[4] e-Math Info Ltd., Dhaka1000, Bangladesh; cmcmath2015@gmail.com
* Correspondence: msh80edu@gmail.com (M.S.H.); mehmetyavuz@erbakan.edu.tr (M.Y.)

Abstract: The present research was developed to find out the effect of heated cylinder configurations in accordance with the magnetic field on the natural convective flow within a square cavity. In the cavity, four types of configurations—left bottom heated cylinder (LBC), right bottom heated cylinder (RBC), left top heated cylinder (LTC) and right top heated cylinder (RTC)—were considered in the investigation. The current mathematical problem was formulated using the non-linear governing equations and then solved by engaging the process of Galerkin weighted residuals based on the finite element scheme (FES). The investigation of the present problem was conducted using numerous parameters: the Rayleigh number ($Ra = 10^3$–10^5), the Hartmann number (Ha = 0–200) at $Pr = 0.71$ on the flow field, thermal pattern and the variation of heat inside the enclosure. The clarifications of the numerical result were exhibited in the form of streamlines, isotherms, velocity profiles and temperature profiles, local and mean Nusselt number, along with heated cylinder configurations. From the obtained outcomes, it was observed that the rate of heat transport, as well as the local Nusselt number, decreased for the LBC and LTC configurations, but increased for the RBC and RTC configurations with the increase of the Hartmann number within the square cavity. In addition, the mean Nusselt number for the LBC, RBC, LTC and RTC configurations increased when the Hartmann number was absent, but decreased when the Hartmann number increased in the cavity. The computational results were verified in relation to a published work and were found to be in good agreement.

Keywords: natural convection; magnetic field; FES; heated cylinder; square cavity

Citation: Hossain, M.S.; Fayz-Al-Asad, M.; Mallik, M.S.I.; Yavuz, M.; Alim, M.A.; Khairul Basher, K.M. Numerical Study of the Effect of a Heated Cylinder on Natural Convection in a Square Cavity in the Presence of a Magnetic Field. *Math. Comput. Appl.* **2022**, *27*, 58. https://doi.org/10.3390/mca27040058

Academic Editor: Gianluigi Rozza

Received: 29 May 2022
Accepted: 4 July 2022
Published: 11 July 2022

1. Introduction

As a mechanism of heat transfer, the natural convective electrical conduction flow of fluid, in accordance with the effect of magnetic field in cavities, has been thoroughly studied by researchers due to its technical importance in engineering applications. The extensive studies of various applications include electronic device cooling, ventilation of rooms, reactor insulation, solar ponds, fire prevention and crystal growth in liquids [1]. By considering this importance, many researchers have conducted many numerical and experimental studies inside the cavities with and without obstacles to research the flow and heat transfer behaviors. Krakov and Nikiforov [2] studied the influence of the vertical magnetic field on thermo-magnetic convection in a square cavity. They showed that the convective flow can have either a one-cell or two-cell structure in the cavity. Steady-state

natural convection in a square cavity using a fully compact higher-order computational method was performed by Kalita et al. [3]. Conjugate gradient and hybrid bi-conjugate gradient are used to find good convergence at higher Rayleigh numbers by solving the symmetrical and non-symmetrical algebraic systems. Natural convection in a square enclosure was performed by Shu and Wee [4] using the SIMPLE-generalized differential quadrature method and produced accurate numerical results only for a few grid points. Basak and Roy [5] examined the thermal effects of natural convection flows within a square cavity. They found that the power law correlations played a vital role between the average Nusselt number and Rayleigh numbers for convection-dominated regimes. Natural convection fluid flow and heat transfer using discrete source–sink pairs in square cavities were studied by Deng [6]. The result showed that total heat transmission is directly proportional to the amount of eddies in the enclosure. Pirmohammadi et al. [7] investigated buoyancy-driven convection and the influence of magnetic field within a differentially heated square cavity. The result indicated that the magnetic field reduces the rate of convective heat transfer. Magneto convection and partially active vertical walls in a square cavity were studied by Nithyadevi et al. [8].

With the increase in the Hartmann number, the average Nusselt number decreased, but the Prandtl number and Grashof number increased. The porous layer on the flow structure and heat transfer within a square was examined by Hamimid et al. [9] to find out the velocity pressure formulation. Jani et al. [10] studied MHD free convection in a square cavity with a hot bottom wall and cooled side walls. It was found that the magnetic field reduced free convection strength as well as flow velocity and at higher Rayleigh numbers. Natural convection with an inner circular cylinder through square enclosure was investigated by Lee et al. [11]. It was found that the size of the local heating zone influenced the production and dissolution of vortices. Hussein et al. [12] studied transient natural convection flow in the enclosures and obtained heat transfer properties of three-dimensional impacts of transitory natural convection. Natural convection in a square cavity was examined by Park et al. [13], where two inner circular cylinders were positioned in the cavity. Hossain et al. [14] performed a trapezoidal cavity, including the effect of the magnetic field as well as non-uniformly heated bottom wall. It was demonstrated that the average and local Nusselt number with the non-uniform heating of the cavity's bottom wall depended on dimensionless parameters, as well as tilt angles. The effect of a perpendicular magnetic field on free convection in a rectangular cavity to solve the resulting boundary value problem was examined by Singh et al. [15]. Park et al. [16] studied natural convection in a square enclosure with four circular cylinders to locate various rectangular positions of the cylinders on the flow and thermal fields. Hossain et al. [17] analyzed magneto-natural convection within trapezoidal cavity and utilized circular block in the cavity and observed that the conduction-dominant region had changed for different angles of Φs. Seo et al. [18,19] investigated flow instability on natural convection in a square enclosure with the aid of four inner cylinders. The effects of the rectangular array cylinder positions in a square enclosure on heat transfer characteristics were highlighted. The effect of buoyancy force by using bottom heating in a square cavity was analyzed by Siddiki et al. [20]. An analysis of the flow of natural convection was conducted by Hossain et al. [21] in a trapezoidal cavity, in which a non-uniformly heated triangular block was used inside the cavity. They observed that the heat transfer rates were significantly affected by tilt angles and heated triangular blocks. Feldman [22] studied the oscillatory instability flow of natural convection in a square enclosure, incorporating a tandem of vertically aligned cylinders.

Hossain et al. [23] demonstrated natural convection in a trapezoidal cavity and also utilized magnetic fields and cold triangular obstacles. They observed that streamlines, isotherms and average Nusselt numbers were affected by rotations of the cold triangular obstruction. Magneto-hydrodynamic free convection through a square enclosure Lattice Boltzmann simulation was studied by Laouer and Djeghiour [24]. It was seen that the heat transfer rate fell as the *Ha* increased, but it increased when the *Ra* increased. Furthermore,

for high Rayleigh numbers and a wide range of Hartmann numbers, the magnetic field direction had a significant impact on the heat transfer and fluid movement inside the enclosure. Fayz-Al-Asad et al. [25] analyzed natural convection in a wavy cavity to obtain the result of the fin length and its location. They found that there was a significant impact on the flow structure and temperature for the fin lengths and their locations. Magneto-hydrodynamic natural convection flow was studied by Hossain et al. [26]. They used heated triangular obstacles in accordance with a porous trapezoidal cavity. They showed that local and average Nusselt numbers were highly influenced by a variety of aspect ratios of heat source obstacles within the cavity. Liao and Li [27] presented an empirical correlation of natural convection with the effect of a magnetic field in a square enclosure to anticipate the heat transfer transition for various values of *Ha* and *Ra*. Shahid et al. [28] studied a lid-driven rectangular cavity using a multi-relaxation time Lattice Boltzmann simulation. They analyzed the aspect ratio of the cavity, as well as the sizes of the heated obstacles on fluid flow. Natural convection flow in a trapezoidal cavity was studied by Khan et al. [29]. They used a porous matrix within the cavity, along with heated cylindrical barriers. They showed that the average Nusselt number showed a dominant boost for both the fluid and solid phases. Fayz-Al-Asad et al. [30,31] studied a vertically wavy enclosure. They used magneto conditions to find out the effect of undulation in the cavity. They observed that, due to the increase in the number of undulations, the evolution of heat transport increased. The study of a rectangular heating source ofnatural convective flow within a triangular cavity was conducted by Fayz-Al-Asad et al. [32]. They confirmed that the rate of heat variation increased as the Rayleigh number increased in the cavity. Fayz-Al-Asad et al. [33] analyzed the magneto-combined convection in a lid-driven wavy cavity. They found that variations of lengths of the fin surface had a significant impact on the flow building and heat line sketch. Mixed convection flow in a lid-driven cavity was performed by Xiong et al. [34] for different obstacles. The results showed that the intensity of maximum convection was achieved for a higher Grashof number. Recently, Alshare et al. [35] conducted a hydrothermal and entropy critique of nanofluid natural convection inside an elliptical shape in the concentric irregular cavity. They observed that a single increase in undulation increased the Nusselt number by an average of 9.5% within the examined range (N = 1 to 4). Furthermore, doubling the nanoparticle volume fraction increased the Nusselt number by nearly 8%. In addition, the finite element method, magnetic field and natural convection were found to be more detailed [36–39].

To the best knowledge of the scientist, it was noted that no inquiry has been conducted on the effect of heated cylinders in accordance with magnetic-natural convection flow in a square cavity in which the geometrical result for the heat transport characteristics is necessary in order to know the industrial functions. The flow field has been characterized by the streamlines whereas the thermal area is defined by the isotherms, local and average Nusselt numbers. For computation, the Prandtl number (Pr = 0.71) is considered for the airflow in the cavity. The present research study was conducted for the assorted configurations of heated cylinders for the range of Ha and *Ra* on flow, as well as thermal field through square enclosure.

2. Problem Definition

The physical configuration for the current investigation is shown in Figure 1. A steady, two-dimensional square cavity with various heated cylinders (LBC, RBC, LTC and RTC) embedded inside, along with magnetic field (B_0) with the y-axis, was used in the present model. The dimension of the cavity was defined by its height (H) and length (L). The gravitational force (g) always worked in the vertically downward direction. The left and right walls of the cavity were thermally insulated (T_i). The base wall of the cavity was considered to be at a uniform hot temperature (T_h) and the top wall was maintained at a cold temperature (T_c), where $T_h > T_c$. Furthermore, a heated cylinder of a diameter D was placed in various positions within the square cavity. The diameter of the cylinder was made to be one third of the cavity's height. The electrically conductive fluid with

Pr = 0.71 [10] was placed in the square cavity and the flow of fluid was thought to be Newtonian and laminar. In addition, stable fluid properties were seen, and the boundary walls of the cavity were no-slip.

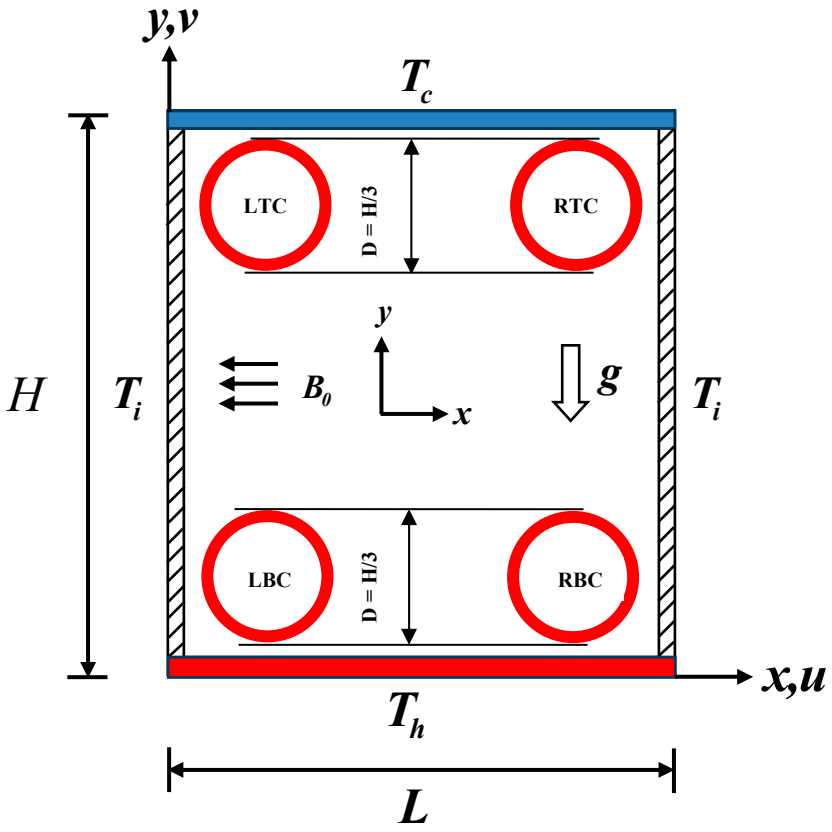

Figure 1. Schematic model of the present study.

3. Mathematical Modeling

The flow of fluid was steady, viscous and incompressible in the present study. The electrically conducting flow of fluid was also invariant, excluding density variation. Furthermore, Boussinesq approximation was used to report the variation of density as a function of temperature and, in this way, connect the temperature field to the flow field for the treatment of buoyancy term in the momentum equation. In addition, viscous dissipation, the effect of radiation, the low-magnetic Reynolds number model for Lorentz force and Joule heating were neglected in this study. The two-dimensional conservations equations of mass, momentum and energy for the present study in dimensionless form were as follows [10,14,17,23,26,40,41]:

$$\frac{\partial U}{\partial X} + \frac{\partial V}{\partial Y} = 0, \tag{1}$$

$$U\frac{\partial U}{\partial X} + V\frac{\partial U}{\partial Y} = -\frac{\partial P}{\partial X} + \mathrm{Pr}\left(\frac{\partial^2 U}{\partial X^2} + \frac{\partial^2 U}{\partial Y^2}\right), \tag{2}$$

$$U\frac{\partial V}{\partial X} + V\frac{\partial V}{\partial Y} = -\frac{\partial P}{\partial Y} + Pr\left(\frac{\partial^2 V}{\partial X^2} + \frac{\partial^2 V}{\partial Y^2}\right) + RaPr\theta - Ha^2PrV, \tag{3}$$

$$U\frac{\partial \theta}{\partial X} + V\frac{\partial \theta}{\partial Y} = \left(\frac{\partial^2 \theta}{\partial X^2} + \frac{\partial^2 \theta}{\partial Y^2}\right). \tag{4}$$

Using the following variables in the present study, Equations (1)–(4) were non-dimensionalized:

$$X = \frac{x}{L},\ Y = \frac{y}{L},\ U = \frac{uL}{\alpha},\ V = \frac{vL}{\alpha},\ P = \frac{pL^2}{\rho\alpha^2},\ \theta = \frac{T-T_c}{T_h-T_c},$$
$$Ha = B_0 L\sqrt{\frac{\sigma}{\mu}},\ Pr = \frac{v}{\alpha},\ Ra = \frac{g\beta(T_h-T_c)L^3}{\alpha v},$$

where X and Y both are non-dimensional coordinates alongside horizontal and vertical directions, respectively; U and V are non-dimensional velocity components in X and Y directions, respectively; θ and P are the non-dimensional temperature and pressure; and Ra, Pr and Ha, are the Rayleigh number, the Prandtl number and the Hartmann number, respectively. Thermal diffusivity, volumetric thermal expansion coefficient, kinematic viscosity, density, specific heat, acceleration due to gravity and dimensional temperature difference of the fluid are represented, respectively, by the symbols α, β, ν, ρ, c_p, g, and ΔT.

The related boundary conditions for Equations (1)–(4) take the following forms:
on the left and right (side) walls: $U = 0,\ V = 0,\ \frac{\partial\theta}{\partial n} = 0$;
on the top wall: $U = 0, V = 0, \theta = 0$;
on the bottom wall: $U = 0, V = 0, \theta = 1$;
on the insider elliptic obstacle: $U = 0, V = 0, \theta = 1$.

The heat transfer co-efficient, as well as the local Nusselt number (Nu_{local}) and mean Nusselt number (Nu_{av}) on the heated part of the cavity, were determined as follows:

$$Nu_{local} = -\frac{\partial\theta}{\partial Y} \text{ and } Nu_{av} = \int_0^1 Nu_{local}\, dX$$

4. Numerical Details

The computational technique was employed to simulate the flow dynamics within the cavity for the problem presented in this paper, with the help of the Galerkin weighted residual finite element technique. Using this technique, the solution domain was discretized into finite element meshes composed of non-uniform triangular elements. Then, the nonlinear governing partial differential equations (i.e., mass, momentum and energy equations) were transferred into a system of integral equations by applying this technique. The Galerkin weighted residual finite element technique (as shown in the works of Taylor and Hood [42], Zienkiewicz [43] and Dechaumphai [44]) was applied to Equations (1)–(4) for the evaluation of finite element equations as:

$$\int_A N_\alpha\left(\frac{\partial U}{\partial X} + \frac{\partial V}{\partial Y}\right)dA = 0, \tag{5}$$

$$\int_A N_\alpha\left(U\frac{\partial U}{\partial X} + V\frac{\partial U}{\partial Y}\right)dA = -\int_A H_\lambda\left(\frac{\partial P}{\partial X}\right)dA + Pr\int_A N_\alpha\left(\frac{\partial^2 U}{\partial X^2} + \frac{\partial^2 U}{\partial Y^2}\right)dA, \tag{6}$$

$$\int_A N_\alpha\left(U\frac{\partial V}{\partial X} + V\frac{\partial V}{\partial Y}\right)dA = -\int_A H_\lambda\left(\frac{\partial P}{\partial Y}\right)dA + Pr\int_A N_\alpha\left(\frac{\partial^2 V}{\partial X^2} + \frac{\partial^2 V}{\partial Y^2}\right)dA + RaPr\int_A N_\alpha\theta dA - Ha^2\int_A N_\alpha V dA, \tag{7}$$

$$\int_A N_\alpha\left(U\frac{\partial\theta}{\partial X} + V\frac{\partial\theta}{\partial Y}\right)dA = \int_A N_\alpha\left(\frac{\partial^2\theta}{\partial X^2} + \frac{\partial^2\theta}{\partial Y^2}\right)dA, \tag{8}$$

where A is the element section; N_α refers to functions of element interpolation for velocity and temperature and α = 1, 2, . . . , 6; H_λ refers to functions of element exclamation for pressure; and λ = 1, 2, 3.

Gauss's theorem with appropriate boundary integral terms, in accordance with heat flux and surface tractions, was applied to Equations (6)–(8), then becoming

$$\begin{array}{c}\int_A N_\alpha\left(U\frac{\partial U}{\partial X}+V\frac{\partial U}{\partial Y}\right)dA+\int_A H_\lambda\left(\frac{\partial P}{\partial X}\right)dA\\ +Pr\int_A\left(\frac{\partial N_\alpha}{\partial X}\frac{\partial U}{\partial X}+\frac{\partial N_\alpha}{\partial Y}\frac{\partial U}{\partial Y}\right)dA=\int_{S_0}N_\alpha S_x dS_0,\end{array} \tag{9}$$

$$\begin{array}{c}\int\limits_A N_\alpha\left(U\frac{\partial V}{\partial X}+V\frac{\partial V}{\partial Y}\right)dA+\int\limits_A H_\lambda\left(\frac{\partial P}{\partial Y}\right)dA\\ +Pr\int\limits_A\left(\frac{\partial N_\alpha}{\partial X}\frac{\partial V}{\partial X}+\frac{\partial N_\alpha}{\partial Y}\frac{\partial V}{\partial Y}\right)-RaPr\int\limits_\alpha N_\alpha\theta dA+Ha^2\int\limits_\alpha N_\alpha V dA=\int\limits_{s_0}N_\alpha S_y dS_0\,,\end{array} \tag{10}$$

$$\int\limits_\alpha N_\alpha\left(U\frac{\partial\theta}{\partial X}+V\frac{\partial\theta}{\partial Y}\right)dA+\int\limits_\alpha\left(\frac{\partial N_\alpha}{\partial X}\frac{\partial\theta}{\partial X}+\frac{\partial N_\alpha}{\partial Y}\frac{\partial\theta}{\partial Y}\right)dA=\int\limits_{S_w}N_\alpha q_{lw}dS_w, \tag{11}$$

where (9)–(10) specify the surface tractions (S_x, S_y) alongside the outflow boundary S_0 and (11) specifies the components of velocity and heat flux (q_w), which flows into or out from field alongside S_w.

Now, the basic unidentified elements for the major partial differential equations are velocity distributions components U and V; the temperature distribution θ; and the pressure distribution P. These distributions, by their uppermost derivative orders, were then applied to Equations (5)–(8):

$$U(X,Y)=N_\beta U_\beta,\ V(X,Y)=N_\beta V_\beta,\ \theta(X,Y)=N_\beta\theta_\beta,\ P(X,Y)=H_\lambda P_\lambda, \tag{12}$$

where $\beta = 1, 2, \ldots, 6$; $\lambda = 1, 2, 3$.

The finite element equations, by substituting Equation (12), are as follows:

$$K_{\alpha\beta^x}U_\beta+K_{\alpha\beta^y}V_\beta=0, \tag{13}$$

$$K_{\alpha\beta\gamma^x}U_\beta U_\gamma+K_{\alpha\beta\gamma^y}V_\gamma U_\gamma+M_{\alpha\mu^x}P_\mu+Pr\left(S_{\alpha\beta^{xx}}+S_{\alpha\beta^{yy}}\right)U_\beta=Q_{\alpha^u}, \tag{14}$$

$$K_{\alpha\beta\gamma^x}U_\beta V_\gamma+K_{\alpha\beta\gamma^y}V_\gamma V_\gamma+M_{\alpha\mu^y}P_\mu+Pr(S_{\alpha\beta^{xx}}+S_{\alpha\beta^{yy}}+Ha^2K_{\alpha\beta})V_\beta-RaPrK_{\alpha\beta}\theta_\beta=Q_{\alpha^v}, \tag{15}$$

$$K_{\alpha\beta\gamma^x}U_\beta\theta_\gamma+K_{\alpha\beta\gamma^y}V_\beta\theta_\gamma+\left(S_{\alpha\beta^{xx}}+S_{\alpha\beta^{yy}}\right)\theta_\beta=Q_{\alpha^\theta}, \tag{16}$$

where element matrices coefficients are in the shape of the integrals in the element region and alongside the element edges S_0 and S_w as:

$$\begin{array}{c}K_{\alpha\beta^x}=\int_A N_\alpha N_{\beta,x}dA,\ K_{\alpha\beta^y}=\int_A N_\alpha N_{\beta,y}dA,\ K_{\alpha\beta\gamma^x}=\int_A N_\alpha N_\beta N_{\gamma,x}dA,\\ K_{\alpha\beta\gamma^y}=\int_A N_\alpha N_\beta N_{\gamma,y}dA,\ K_{\alpha\beta}=\int_A N_\alpha N_\beta dA,\ S_{\alpha\beta^{xx}}=\int_A N_{\alpha,x}N_{\beta,x}dAS_{\alpha\beta^{yy}}=\int_A N_{\alpha,y}N_{\beta,y}dA,\\ M_{\alpha\mu^x}=\int_A H_\alpha H_{\mu,x}dA,\ M_{\alpha\mu^y}=\int_A H_\alpha H_{\mu,y}dA,\\ Q_{\alpha^u}=\int_{S_0}N_\alpha S_x dS_0,\ Q_{\alpha^v}=\int_{S_0}N_\alpha S_y dS_0,\ Q_{\alpha^\theta}=\int_{S_w}N_\alpha q_{1w}dS_w, Q_{\alpha^\theta s}=\int_{S_w}N_\alpha q_{2w}dS_w.\end{array}$$

The non-linear resulting finite element Equations (13)–(16) are algebraic. Finally, the process of Newton–Raphson, as well as the integration technique, was used to iteratively determine the equations of residuals. A convergence of the procedure of computation is put aside once the convergence criteria or the condition is determined as $\left|\frac{\Psi^{n+1}-\Psi^n}{\Psi^{n+1}}\right|<10^{-6}$, where n refers to the iterative number, $\psi=\psi(U,\ V,\theta)$.

As the code validation is necessary for the accurateness of the numerical technique, the present problem is considered with $Pr = 0.71$, $Ha = 50$ and $Ra = 10^5$, which had been solved for streamlines (stream function) and isotherms for 2D magneto-hydrodynamic free convection flow through the square cavity. The result was checked for streamlines and isotherms and then the present work was compared with the reported reference of Jani et al. [10] and presented in Figure 2. From the above comparisons of the figures, we found a good agreement between the present work and Jani et al. [10], which is displayed in Figure 2. Furthermore, mesh configuration is a technique in which a large domain is subdivided into a set of sub domains called finite elements, control volume and so on. A lot

of boundary value problems of several engineering fields have been solved with the aid of irregular geometry via a set of finite elements. The answer for the current geometry for the specific non-dimensional parameters was computed at discrete locations called numerical grids. The mesh structure for the current problem is provided in Figure 3.

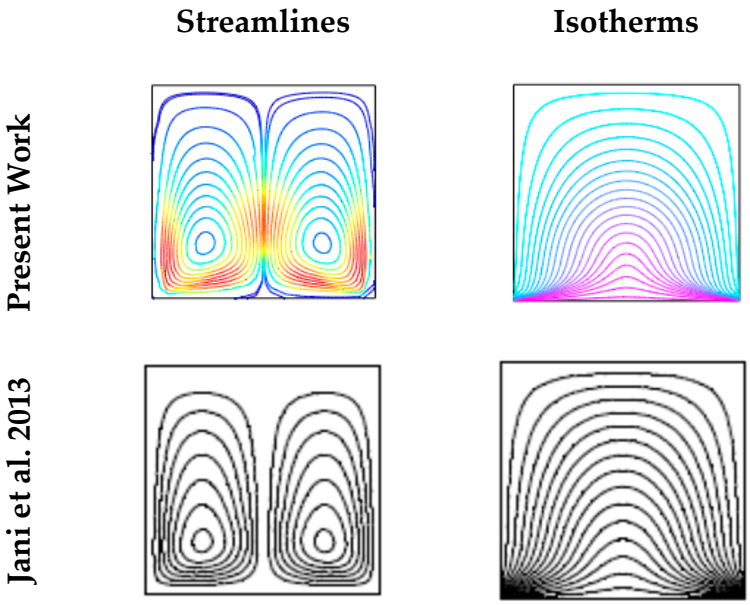

Figure 2. Comparison of streamlines and isotherms of by Jani et al. [10] and the present work with $Pr = 0.71$, $Ha = 50$ and $Ra = 10^5$.

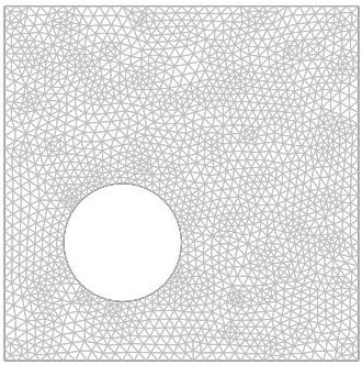

Figure 3. Mesh configuration for the cavity.

In addition, to select a proper grid size, in the present study, a particular grid sensitivity selecting procedure was performed for the square cavity along with various heated cylinders for $Pr = 0.71$, $Ha = 100$ and $Ra = 10^5$, considering assorted size of mesh. The manifest meshing is shown in Table 1 and Figure 4, where the average Nusselt number is calculated. It was found that further increments of Nu_{av} have insignificant transform. Throughout the study, for 23,780 nodes and 3568 elements, the mesh configuration was chosen for accurate simulation to find the optimized, desired result in the present study.

Table 1. Grid sensitivity tests at $Pr = 0.71$, $Ha = 100$ and $Ra = 10^5$.

Nodes	16,030	19,099	21,560	23,780	32,945	37,682
Elements	2408	2878	3258	3568	4978	5696
Nu_{av}	0.130212	0.130203	0.137988	0.141502	0.141502	0.1415
Time (s)	15.913	19.308	22.568	26.879	36.5135	38.495

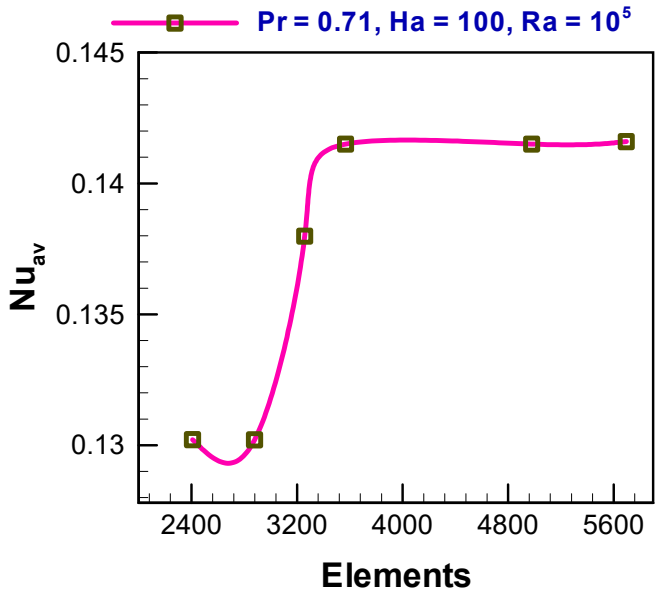

Figure 4. Grid sensitivity tests for $Pr = 0.71$, $Ha = 100$ and $Ra = 10^5$.

5. Results and Discussion

In the present study, the effect of a heated cylinder for different configurations, LBC, RBC, LTC and RTC, in accordance with the magnetic field for the fluid flow on the natural convection in a square cavity numerically, was studied. The results of the square cavity with an insider heated cylinder were presumed for electrically conductive fluid with the Prandtl number ($Pr = 0.71$) and a confined airflow. The wide range of governing parameters were the Rayleigh number ($10^3 \leq Ra \leq 10^5$) and the Hartmann number ($0 \leq Ha \leq 200$), studied here in order to find the computational results. The results were analyzed in the form of streamlines and isotherms, velocity profiles, temperature profiles, heat transfer rates and local and mean Nusselt numbers, alongside the heated wall of the cavity.

5.1. Effect of Cylinder Position and Magnetic Field on Streamlines and Isotherms

Streamlines and isotherms for assorted heated cylinder configurations along with different parameters *Ha*, *Pr* and *Ra* were shown in Figures 5–8. As the beneath wall of the cavity and cylindrical block were heated, the flow of hot fluids creates eddy circulation cells, rotating along the cold walls inside the cavity from the heating wall for all parameters: *Pr*, *Ha* and *Ra*. To find the variations of streamlines and isotherms on various configurations of heated cylinders (LBC, RBC, LTC and RTC), a numerical study was performed with $Pr = 0.71$, $Ha = 0$–200 and $Ra = 10^3$–10^4, correspondingly, for flow and thermal field in Figures 5 and 6. The impact of the presence of a magnetic field for streamlines and isotherms is also demonstrated in Figures 5a and 6, respectively, for cavity configuration (LBC). Figure 5a shows that one eddy circulation cell formed inside the cavity. The flow strength decreases and streamlines close to the heated cylinder configurations due to the enhancement of the Hartmann number, which is shown in Figure 5b–d. The effect of the Hartmann number ($Ha = 0$–200) on the distributions of the velocity and temperature contours for right bottom configuration (RBC), while $Ra = 10^3$ and $Pr = 0.71$ is also shown in Figure 5. A tiny recirculation cell appeared in the center of the square of the cavity and the recirculation cell was smaller, owing to the increase in the Hartmann number, which is shown in Figure 5. Figure 5 also illustrates the streamlines for the left top heated cylinder configurations (LTC), along with variations of the Hartmann number ($Ha = 0$–200), when $Ra = 10^3$ and $Pr = 0.71$. Figure 5 shows in the LTC configuration that one cell was created inside the center of the square cavity in the absence of magnetic field. In addition to this, one large vortex also formed in the left bottom side of the cavity. The cell became bigger and oval shaped in the cavity with the increase of the Hartmann number and also, a tiny

vortex was found in the left top side of the cavity. The variation of the Hartmann number for the right top cylindrical heat source (RTC) configuration is shown in Figure 5 for the square cavity. It can be seen that the smaller cell was formed in the square cavity due to both the absence and presence of Ha, compared with the LTC. Figure 6 shows that the isotherms for the left bottom heated cylinder configuration (LBC) are likely linear, as well as nonlinear close to the upper wall and base wall, correspondingly, with the increase in the Hartmann number when $Ra = 10^3$ and $Pr = 0.71$ (see Figure 6a–d). Furthermore, Figure 6a–d shows the thermal increases, owing to the increase of the magnetic field parameter: the Hartmann number (Ha). The temperature distributions for the right bottom cylindrical heat source configuration (RBC) with magnetic field's effect on the parameter Hartmann number (Ha = 0–200) is shown in Figure 6a–d for fixed $Ra = 10^3$ and $Pr = 0.71$. The isotherms were parallel to the upper wall of the cavity. On the other hand, a nonlinearity effect was found near to the base wall of the cavity. The isotherms for LTC shown in Figure 6 were almost as linear as those near to the top wall. However, bend isotherms could be seen near the base wall through the effect of the Hartmann number. By increasing the Hartmann number, it could be seen that the isotherms in the RTC transform slightly in the cavity, as shown in Figure 6. When the Rayleigh number increased, that is, for higher $Ra = 10^5$, streamlines and isotherms were analyzed, as shown in Figures 7 and 8 for various configurations of heated cylinders (LBC, RBC, LTC and RTC) within the square cavity for Ha = 0–200 and $Pr = 0.71$. As shown in Figure 7, by analyzing all configurations of the heated cylinders (LBC, RBC, LTC and RTC), it can be understood that one primary larger eddy circulation cell was created inside the cavity when $Ha = 0$. However, due to the increase in the Hartmann number ($0 \leq Ha \leq 200$), the velocity flow strength dwindled. Therefore, likely larger secondary recirculation cells with tiny vortices were created inside the square cavity. At higher $Ra = 10^5$–10^3 and when $Pr = 0.71$, it is shown in Figure 8 that isotherms for every arrangement of heated cylinders (LBC, RBC, LTC and RTC) looked parallel and non-parallel, respectively, near to the upper and beneath wall of the cavity for the impact of magnetic field Ha = 0–200. However, due to the increased Hartmann number and strength of flow of convection, more compacted and non-parallel isotherm lines were seen in the cavity. In addition to this, fewer bond isotherm lines were also observed near the side walls of the cavity.

5.2. Velocity and Temperature Profiles

Figure 9 displays the effects of the Hartmann number (Ha) on velocity pro-files with distances for different cylinder configurations (LBC, RBC, LTC and RTC) adjacent to the line X = 0.3. As shown in Figure 9, the velocity decreased for each cylinder configuration (LBC, RBC, LTC and RTC) and with the increasing value of the Hartmann number below the central portion of the cavity. On the other hand, the velocity increased with the decrease in the Hartmann number. Due to the counterclockwise and clockwise flow directions, the maximum and minimum velocities were found in the absence of a magnetic field. The temperature fields with the distance X are plotted in Figure 10 for different cylinder heat source configurations (LBC, RBC, LTC and RTC). Figure 10 shows, for LBC, RBC, LTC and RTC, that when the Hartmann number was absent, the maximum and minimum temperatures were found in the cavity. The temperature field lessened due to the increase in the Hartmann number. For LBC and LTC, the temperature field transformed slightly with the increase in the Hartmann number to $X < 0.2$, but transformed significantly when the Hartmann number was $X > 0.2$. An inverse result was observed for RBC and RTC. It was observed that the change in the temperature field was insignificant when the Hartmann number increased to $X < 0.4$, but the change was significant when the Hartmann number was $X > 0.4$.

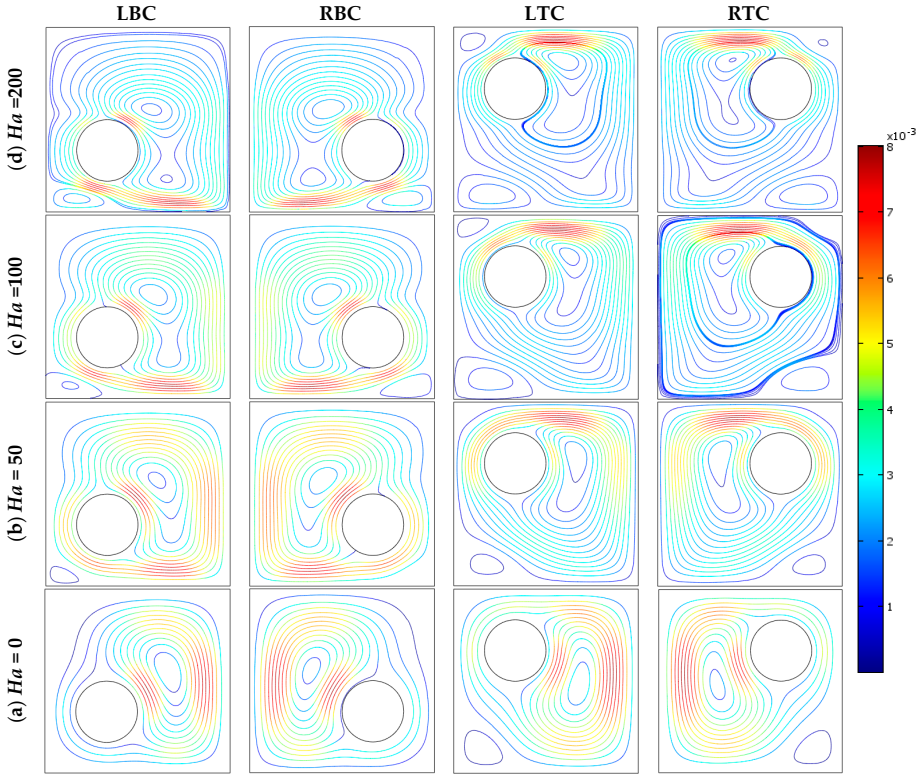

Figure 5. Streamlines for different orientations of heated cylinders for Ha = 0–200, Ra = 10^3 and Pr = 0.71.

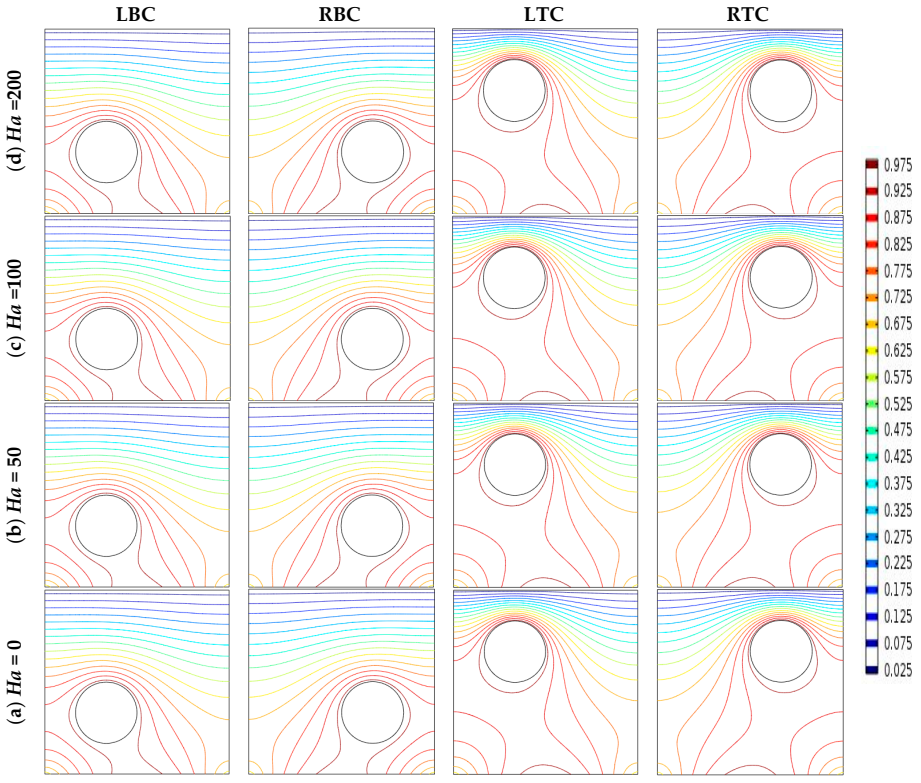

Figure 6. Isotherms for different orientations of heated cylinders for Ha = 0–200, Ra = 10^3 and Pr = 0.71.

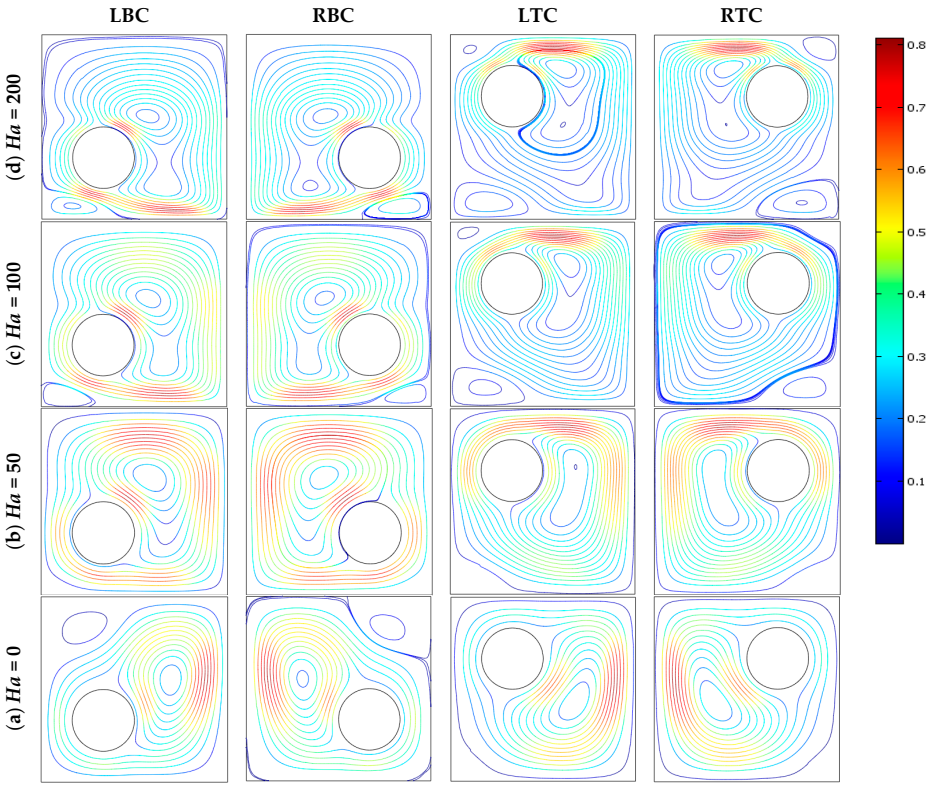

Figure 7. Streamlines for different orientations of heated cylinders for Ha = 0–200, Ra = 10^5 and Pr = 0.71.

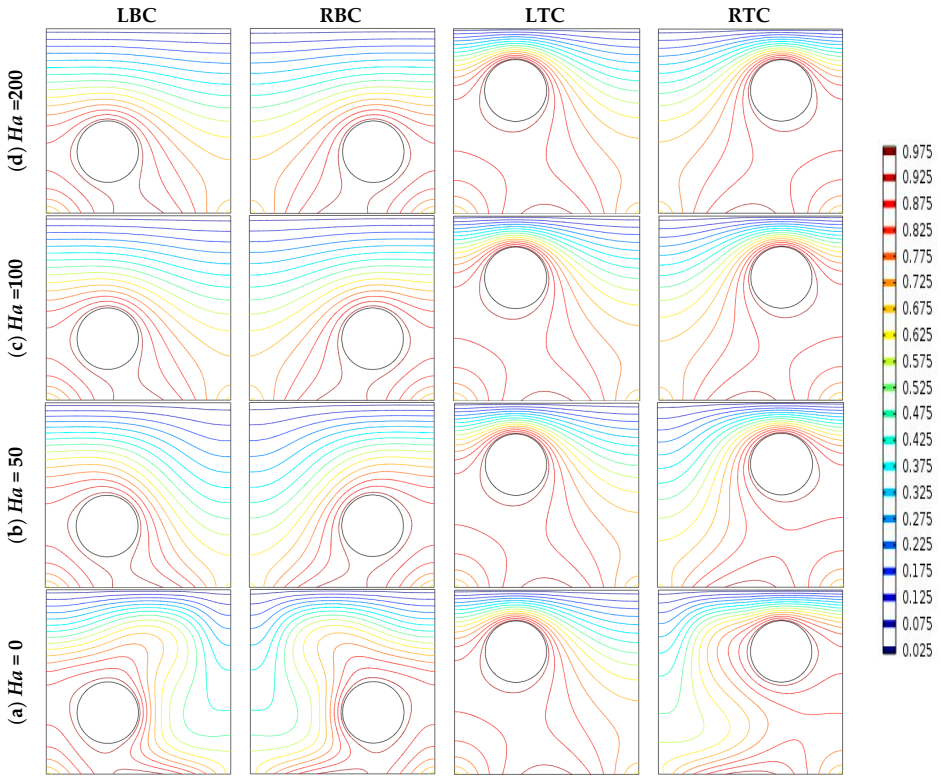

Figure 8. Isotherms for different orientations of heated cylinders for Ha = 0–200, Ra = 10^5 and Pr = 0.71.

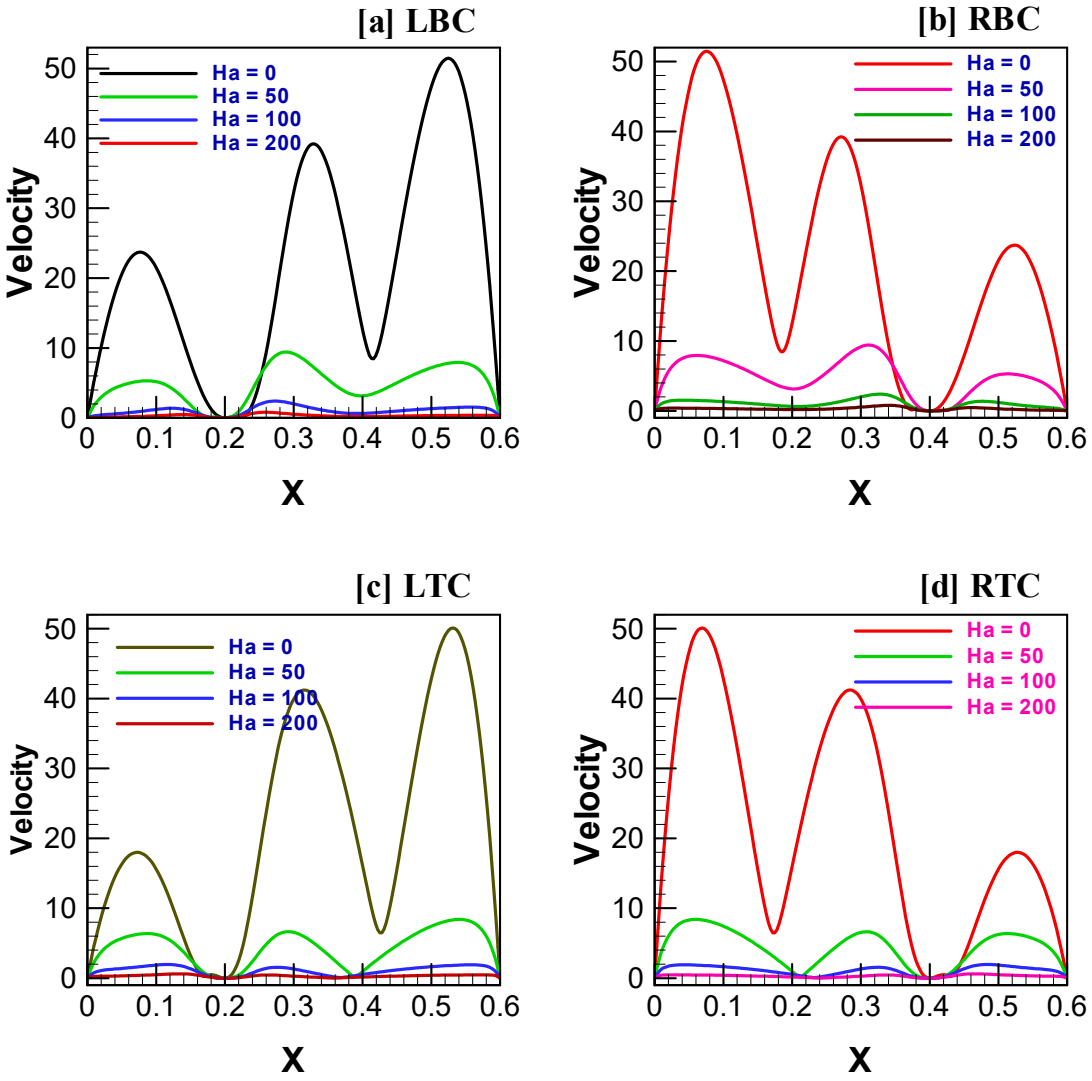

Figure 9. Variations of velocity vs. distance for different orientations of heated cylinders for Ha = 0–200, $Ra = 10^5$ and Pr = 0.71.

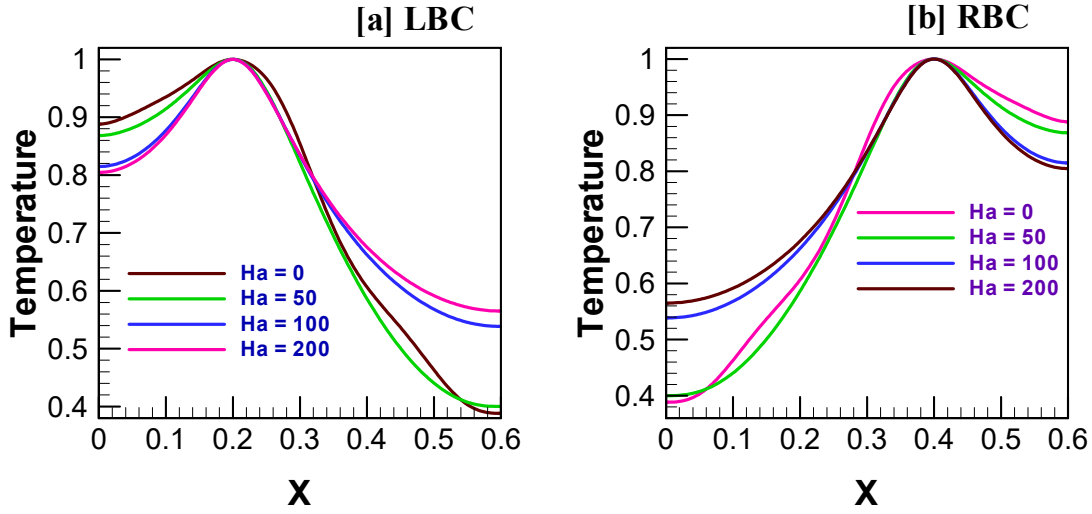

Figure 10. *Cont.*

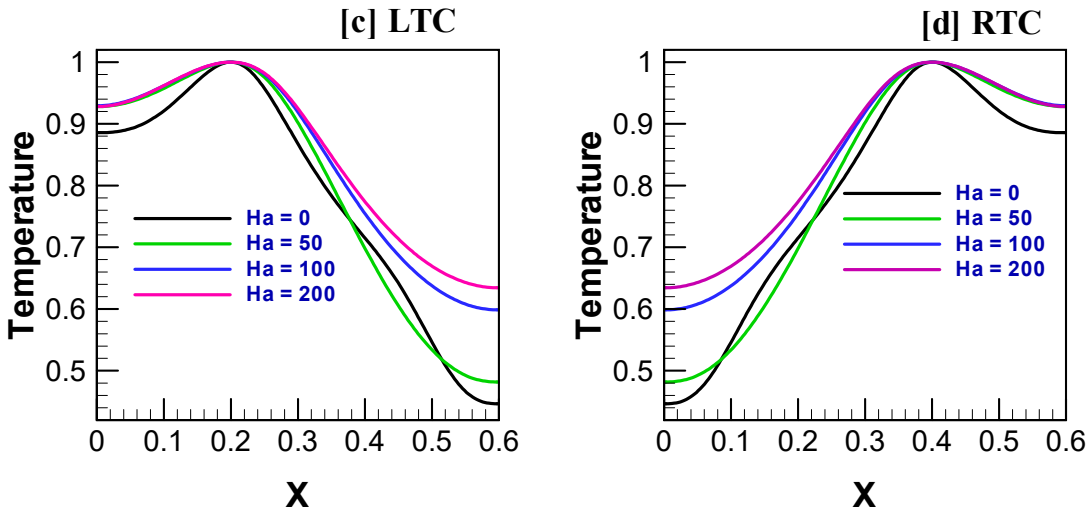

Figure 10. Variations of temperature with distance for different orientations of heated cylinders for Ha = 0–200, $Ra = 10^5$ and Pr = 0.71.

5.3. Heat Transfer

The heat transfer rates, as well as the local Nusselt number with the distance wall for different configurations (LBC, RBC, LTC and RTC) are presented in Figure 11 for the variations of the Hartmann number. Regarding the LBC and LTC configurations, Figure 11 shows that the local Nusselt number decreased with the increase in the Hartmann number, but for the RBC and RTC configurations, it was observed that the local Nusselt number increases due to the increasing Hartmann number. The heat transfer rates, as well as the mean Nusselt number for different configurations (LBC, RBC, LTC and RTC) are presented in Figure 12 against the variations of the Hartmann number. Figure 12 shows, for all configurations, that the mean Nusselt number increases due to the absence of the Hartmann number, but the mean Nusselt number decreases due to the increase in the Hartmann number.

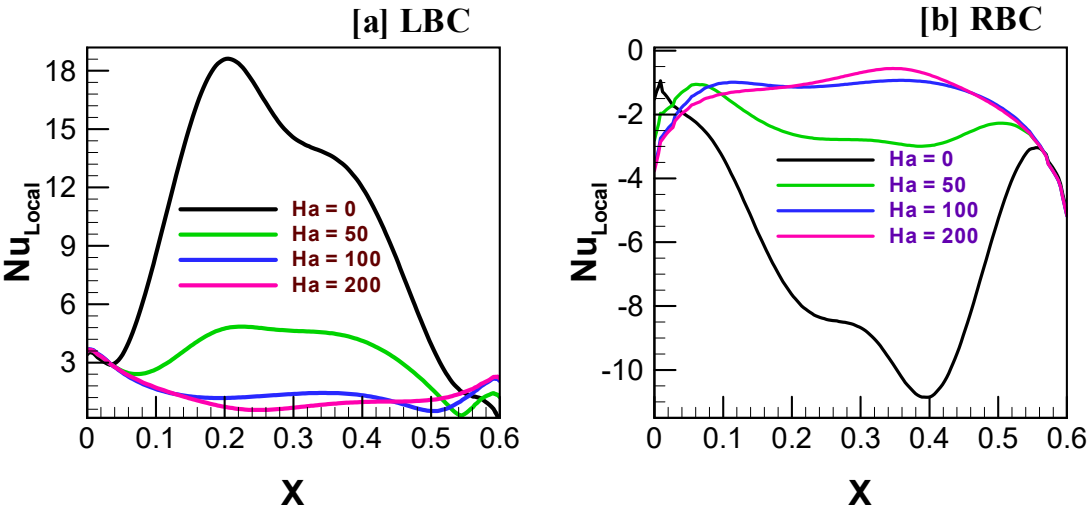

Figure 11. *Cont.*

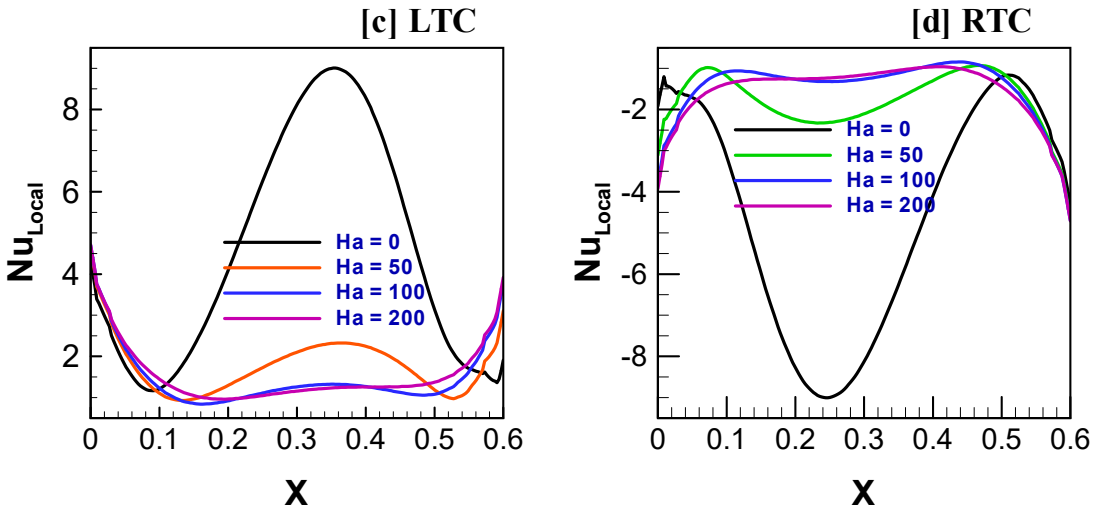

Figure 11. Variations of local Nusselt number with distance for different orientations of heated cylinders for Ha = 0–200, $Ra = 10^5$ and Pr = 0.71.

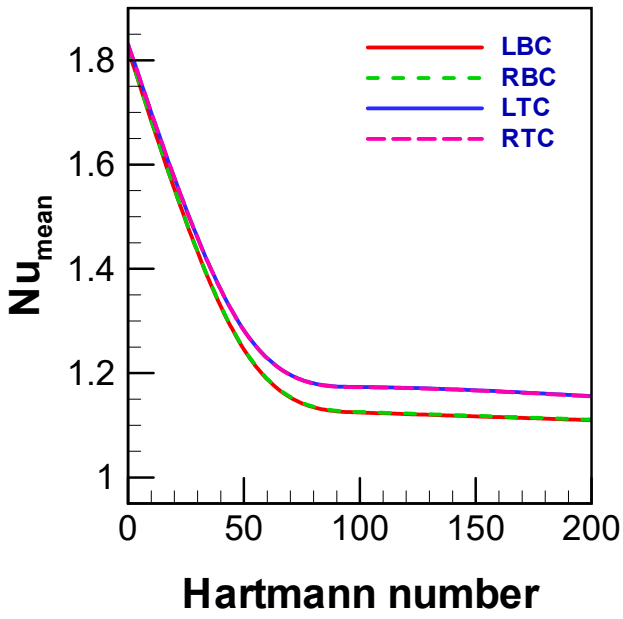

Figure 12. Variations of average Nusselt number with the Hartmann number for different orientations of heated cylinders for Ha = 0–200, $Ra = 10^5$ and Pr = 0.71.

6. Conclusions

A 2D computational framework was generated to analyze the fluid dynamic performance in a square cavity in order to find the effect of heating cylinders in line with a magnetic field using natural convection by applying the free triangular grid-established finite element technique through the use of an easy algorithm. The numerical work within a square cavity for various cylindrical heat source configurations (LBC, RBC, LTC and RTC) when $Pr = 0.7$, $0 \leq Ha \leq 200$ and $10^3 \leq Ra \leq 10^5$ was studied in this work by employing the Galerkin weighted residual method of finite element formulation. The results are displayed for assorted cylinder configurations in the phase of streamlines, isotherms, velocity profiles, temperatures and heat transfers rates, as well as the local and mean Nusselt number for the bottom wall of the cavity. The concise summary is as follows:

- The distributions of flow field and isotherm patterns, velocity and temperature profiles, rate of heat transport for various cylinder configurations within the cavity fully

depended on the Prandlt number (*Pr*), the Rayleigh number (*Ra*) and the Hartmann number (*Ha*) and the heated bottom wall of the cavity.
- The number of vortices increased within the streamlines for various configurations of the cavity due to enhance of the Hartmann number.
- The bonding of isotherm lines reduced close to the side walls of the cavity.
- The bend isotherm lines were observed adjacent to the base wall of the cavity.
- The velocity decreased for each heated cylinder configurations (LBC, RBC, LTC and RTC), as well as for the increasing value of the Hartmann number below the central portion of the cavity, but the velocity increased with the decrease in the Hartmann number.
- For the LBC and LTC configurations, the local Nusselt number decreased with the increase of the Hartmann number, but for the RBC and RTC configurations, the local Nusselt number increased with the increase in the Hartmann number.
- The mean Nusselt number for the LBC, RBC, LTC and RTC configurations increased due to the absence of the Hartmann number, but the mean Nusselt number decreased due to the increase in the Hartmann number.

Author Contributions: Conceptualization, visualization, software implementation, methodology, investigation, writing—original draft and editing: M.S.H.; writing—review, methodology, administration and supervision: M.A.A. and M.Y.; writing—review and editing: M.F.-A.-A. and M.S.I.M.; formal analysis: M.S.H. and M.F.-A.-A.; visualization: K.M.K.B. All authors have read and agreed to the published version of the manuscript.

Funding: This research received no external funding.

Acknowledgments: All authors want to express thankfulness to everyone for contribution to accomplish this research work.

Conflicts of Interest: The authors declare no conflict of interest.

Nomenclature

B_0	Magnetic field
Cp	Specific heat at constant pressure (J/kg·K)
g	Gravitational acceleration (m/s^2)
h	Convective heat transfer coefficient (W/m^2·K)
Ha	Hartmann number
k	Thermal conductivity of fluid (W/m·K)
K	Thermal conductivity ratio fluid
N	Non-dimensional distance
Nu_{av}	Mean Nusselt number
Nu_{local}	Local Nusselt number
P	Non-dimensional pressure
p	Pressure
Pr	Prandtl number
Ra	Rayleigh number
T	Non-dimensional temperature
U	Dimensionless horizontal velocity
u	Velocity in x-direction (m/s)
V	Dimensionless vertical velocity
v	Velocity in y-direction (m/s)
x, y	Cartesian coordinates
X, Y	Dimensionless Cartesian coordinates
Greek symbols	
α	Thermal diffusivity (m^2/s)
β	Coefficient of thermal expansion (K^{-1})
θ	Temperature of fluid
$\Delta\theta$	Discrepancy of temperature

μ	Dynamic viscosity of the fluid (Pa·s)
ν	Kinematic viscosity of the fluid (m^2/s)
r	Fluid density (kg/m^3)
σ	Fluid electrical conductivity ($\Omega^{-1}m^{-1}$)
Abbreviations	
LBC	Left bottom heated cylinder
LTC	Left top heated cylinder
RTC	Right top heated cylinder
RBC	Right bottom heated cylinder

References

1. Ostrach, S. Natural convection in enclosure. *ASME J. Heat Transf.* **1988**, *110*, 1175–1190. [CrossRef]
2. Krakov, M.S.; Nikiforov, I.V. Influence of vertical uniform outer magnetic field on thermomagnetic convection in square cavity. *Magnetohydrodynamics* **2001**, *21*, 125–145. [CrossRef]
3. Kalita, J.C.; Dalal, D.C.; Dass, A.K. Fully Compact Higher-Order Computation of Steady-State Natural Convection in a Square Cavity. *Phys. Rev. E* **2001**, *64*, 066703. [CrossRef] [PubMed]
4. Shu, C.; Wee, K.H.A. Numerical Simulation of Natural Convection in a Square Cavity by SIMPLE-Generalized Differential Quadrature Method. *Comput. Fluids* **2002**, *31*, 209–226. [CrossRef]
5. Basak, T.; Roy, S.; Balakrishnan, A.R. Effects of thermal boundary conditions on natural convection flows within a square cavity. *Int. J. Heat Mass Transf.* **2006**, *49*, 4525–4535. [CrossRef]
6. Deng, Q. Fluid flow and heat transfer characteristics of natural convection in square cavities due to discrete source–sink pairs. *Int. J. Heat Mass Transf.* **2008**, *51*, 5949–5957. [CrossRef]
7. Pirmohammadi, M.; Ghassemi, M.; Sheikhzadeh, G.A. Effect of a Magnetic Field on Buoyancy-Driven Convection in Differentially Heated Square Cavity. *IEEE Trans. Magn.* **2009**, *45*, 407–411. [CrossRef]
8. Nithyadevi, N.; Kandaswamy, P.; Sundari, S.M. Magnetoconvection in a square cavity with partially active vertical walls: Time periodic boundary condition. *Int. J. Heat Mass Transf.* **2009**, *52*, 1945–1953. [CrossRef]
9. Hamimid, S.; Guellal, M.; Amroune, A.; Zeraibi, N. Effect of a Porous Layer on the Flow Structure and Heat Transfer in a Square Cavity. *Fluid Dyn. Mater. Process.* **2012**, *8*, 69–90. [CrossRef]
10. Jani, S.; Mahmoodi, M.; Amini, M. Magnetohydrodynamic Free Convection in a Square Cavity Heated from Below and Cooled from Other Walls. *Int. J. Mech. Ind. Sci. Eng.* **2013**, *7*, 750–755. [CrossRef]
11. Lee, H.; Doo, J.; Ha, M.; Yoon, H. Effects of thermal boundary conditions on natural convection in a square enclosure with an inner circular cylinder locally heated from the bottom wall. *Int. J. Heat Mass Transf.* **2013**, *65*, 435–450. [CrossRef]
12. Hussein, A.K.; Awad, M.M.; Kolsi, L.; Fathinia, F.; Adegun, I.K. A comprehensive review of transient natural convection flow in enclosures. *J. Basic Appl. Sci. Res.* **2014**, *11*, 17–27.
13. Park, Y.; Ha, M.; Choi, C.; Park, J. Natural convection in a square enclosure with two inner circular cylinders positioned at different vertical locations. *Int. J. Heat Mass Transf.* **2014**, *77*, 501–518. [CrossRef]
14. Hossain, M.S.; Alim, M.A. MHD free convection within trapezoidal cavity with non-uniformly heated bottom wall. *Int. J. Heat Mass Transf.* **2014**, *69*, 327–336. [CrossRef]
15. Singh, A.K.; Chandran, P.; Sacheti, N.C. Effect of perpendicular magnetic field on free convection in a rectangular cavity. *Sultan Qaboos Univ. J. Sci.* **2015**, *20*, 49–59. [CrossRef]
16. Park, Y.G.; Ha, M.Y.; Park, J. Natural convection in a square enclosure with four circular cylinders positioned at different rectangular locations. *Int. J. Heat Mass Transf.* **2015**, *81*, 490–511. [CrossRef]
17. Hossain, M.S.; Alim, M.A.; Kabir, K.H. Numerical Analysis on MHD Natural Convection within Trapezoidal Cavity Having Circular Block. *Am. J. Appl. Math. Stat.* **2016**, *4*, 161–168. [CrossRef]
18. Seo, Y.M.; Park, Y.G.; Kim, M.; Yoon, H.S.; Ha, M.Y. Two-dimensional flow instability induced by natural convection in a square enclosure with four inner cylinders. part i: Effect of horizontal position of inner cylinders. *Int. J. Heat Mass Transf.* **2017**, *113*, 1306–1318. [CrossRef]
19. Seo, Y.M.; Mun, G.S.; Park, Y.G.; Ha, M.Y. Two-dimensional flow instability induced by natural convection in a square enclosure with four inner cylinders. part ii: Effect of various positions of inner cylinders. *Int. J. Heat Mass Transf.* **2017**, *113*, 1319–1331. [CrossRef]
20. Siddiki, M.N.A.A.; Habiba, F.; Chowdhury, R. Effect of Buoyancy Force on the Flow Field in a Square Cavity with Heated from Below. *Int. J. Discret. Math.* **2017**, *2*, 43–47. [CrossRef]
21. Hossain, M.S.; Alim, M.A.; Andallah, L.S. Numerical Investigation of Natural Convection Flow in a Trapezoidal Cavity with Non-uniformly Heated Triangular Block Embedded Inside. *J. Adv. Math. Comput. Sci.* **2018**, *28*, 1–30. [CrossRef]
22. Feldman, Y. Oscillatory instability of 2D natural convection flow in a square enclosure with a tandem of vertically aligned cylinders. *Fluid Dyn.* **2018**, *50*, 51–410. [CrossRef]
23. Hossain, M.S.; Alim, M.A.; Andallah, L.S. A comprehensive analysis of natural convection in a trapezoidal cavity with magnetic field and cooled triangular obstacle of different orientations. *AIP Conf. Proc.* **2019**, *2121*, 030003. [CrossRef]

24. Laouer, A.; Djeghiour, R. Lattice Boltzmann Simulation of Magnetohydrodynamic Free Convection in a Square Enclosure with Non-uniform Heating of the Bottom Wall. *J. Adv. Res. Fluid Mech. Therm. Sci.* **2019**, *59*, 13–28.
25. Fayz-Al-Asad, M.; Munshi, M.J.H.; Sarker, M.M.A. Effect of fin length and location on natural convection heat transfer in a wavy cavity. *Int. J. Sci. Tech.* **2020**, *7*, 070303. [CrossRef]
26. Hossain, M.S.; Alim, M.A.; Andallah, L.S. Numerical Simulation of MHD Natural Convection Flow Within Porous Trapezoidal Cavity With Heated Triangular Obstacle. *Int. J. Appl. Comput. Math.* **2020**, *6*, 166. [CrossRef]
27. Liao, C.; Li, W. Assessment of the magnetic field influence on heat transfer transition of natural convection within a square cavity. *Case Stud. Therm. Eng.* **2021**, *28*, 101638. [CrossRef]
28. Shahid, H.; Yaqoob, I.; Khan, W.A.; Aslam, M. Multi relaxation time Lattice Boltzmann analysis of lid-driven rectangular cavity subject to various obstacle configurations. *Int. Commun. Heat Mass Transf.* **2021**, *129*, 105658. [CrossRef]
29. Khan, Z.H.; Hamid, M.; Khan, W.A.; Sun, L.; Liu, H. Thermal non-equilibrium natural convection in a trapezoidal porous cavity with heated cylindrical obstacles. *Int. Commun. Heat Mass Transf.* **2021**, *126*, 105460. [CrossRef]
30. Fayz-Al-Asad, M.; Alam, M.N.; Rashad, A.M.; Sarker, M.M.A. Impact of undulation on magneto-free convective heat transport in an enclosure having vertical wavy sides. *Int. Commun. Heat Mass Transf.* **2021**, *127*, 105579. [CrossRef]
31. Fayz-Al-Asad, M.; Alam, M.N.; Tunç, C.; Sarker, M.M.A. Heat transport exploration of free convection flow inside enclosure having vertical wavy walls. *J. Appl. Comput.* **2021**, *7*, 520–527. [CrossRef]
32. Fayz-Al-Asad, M.; Alam, M.N.; Ahmad, H.; Sarker, M.M.A.; Alsulami, M.D.; Gepreel, K.A. Impact of a closed space rectangular heat source on natural convective flow through triangular cavity. *Results Phys.* **2021**, *23*, 104011. [CrossRef]
33. Fayz-Al-Asad, M.; Yavuz, M.; Alam, M.N.; Sarker, M.M.A.; Bazighifan, O. Influence of Fin Length on Magneto-Combined Convection Heat Transfer Performance in a Lid-Driven Wavy Cavity. *Fractal Fract.* **2021**, *5*, 107. [CrossRef]
34. Xiong, P.Y.; Hamid, A.; Iqbal, K.; Irfan, M. Numerical simulation of mixed convection flow and heat transfer in the lid-driven triangular cavity with different obstacle configurations. *Int. Commun. Heat Mass Transf.* **2021**, *123*, 105202. [CrossRef]
35. Alshare, A.; Abderrahmane, A.; Guedri, K.; Younis, O.M.; AliH, M.; Al-Kouz, W. Hydrothermal and Entropy Investigation of Nanofluid Natural Convection in a Lid-Driven Cavity Concentric with an Elliptical Cavity with a Wavy Boundary Heated from Below. *Nanomaterials* **2022**, *12*, 1392. [CrossRef]
36. Asad, M.F.A.; Hosssain, A.; Sarker, M.M.A. Numerical investigation of MHD mixed convection heat transfer having vertical fin in a lid-driven square cavity. *AIP Conf. Proc.* **2019**, *2121*, 030023. [CrossRef]
37. Versaci, M.; Jannelli, A.; Morabito, F.C.; Angiulli, G. A semi-linear elliptic model for a circular membrane MEMS device considering the effect of the fringing field. *Sensors* **2021**, *21*, 5237. [CrossRef]
38. Islam, T.; Yavuz, M.; Parveen, N.; Fayz-Al-Asad, M. Impact of Non-Uniform Periodic Magnetic Field on Unsteady Natural Convection Flow of Nanofluids in Square Enclosure. *Fractal Fract.* **2022**, *6*, 101. [CrossRef]
39. Fayz-Al-Asad, M.; Sarker, M.M.A.; Munshi, M.J.H. Numerical investigation of natural convection flow in a hexagonal enclosure having vertical fin. *J. Sci. Res.* **2019**, *11*, 173–183. [CrossRef]
40. Sene, N. Second-grade fluid with Newtonian heating under Caputo fractional derivative: Analytical investigations via Laplace transforms. *Math. Model. Numer. Simul. Appl.* **2022**, *2*, 13–25. [CrossRef]
41. Yavuz, M.; Sene, N.; Yıldız, M. Analysis of the influences of parameters in the fractional second-grade fluid dynamics. *Mathematics* **2022**, *10*, 1125. [CrossRef]
42. Taylor, C.; Hood, P. A numerical Solution of the Navier-Stokes Equations Using Finite Element Technique. *Comput. Fluids* **1973**, *1*, 73–100. [CrossRef]
43. Zienkiewicz, O.C.; Taylor, R.L. *The Finite Element Method*, 4th ed.; McGraw-Hill: New York, NY, USA, 1991.
44. Dechaumphai, P. *Finite Element Method in Engineering*, 2nd ed.; Chulalongkorn University Press: Bangkok, Thailand, 1999.